Final Technical Report for Award Award G16AP00024

The Dynamics of Earthquakes and Tsunamis along the Alaskan-Aleutian Subduction Zone: Collaborative Research with the University of California, Riverside, and the US Geological Survey

Kenny Ryan
US Geological Survey
345 Middlefield Rd.
Menlo Park CA 94025-3561
650-329-5065
kryan@usgs.gov

David D. Oglesby
Professor of Geophysics
Chair, Department of Earth Sciences
University of California, Riverside
Riverside, CA 92521-0423
PH: (951) 827-2036
david.oglesby@ucr.edu

Eric Geist
US Geological Survey
345 Middlefield Rd.
Menlo Park CA 94025-3561
650-329-5457
egeist@usgs.gov

Term covered: 01/01/2016-06/30/2017

ABSTRACT

We implement stochastic stresses on dip-slip faults based on a modified version of the method of Andrews and Barall (2011) and Andrews and Ma (2016). Specifically, we generate a distribution of complex random amplitudes based on a Gaussian distribution. We then modify those amplitudes such that the amplitudes associated with longer wavelengths are the most prominent. The amplitudes are then filtered to prevent spatial aliasing (i.e., incorrect short wavelength amplitudes) and used to generate a shear stress distribution for a fault. Such shear stress parameterizations are then used as an initial condition for dynamic rupture models, and we implement multiple parameterizations for dynamic earthquake models offshore Alaska. This is an expansion of previous work involving a potential Mw 9 megathrust earthquake and resulting tsunami near the Alaska Peninsula (Ryan et al., 2013). Additionally, we are studying effects on slip distributions due to stochastic fault stress with a free surface boundary condition. In particular, such parameterizations tend to move slip patches somewhat updip of highly prestressed patches, and this likely results from dynamic normal stress perturbations as the rupture

travels updip. Lastly, we are interested in the dynamic slip spectrum that is produced as a result of these initial shear stress distributions. We find that the resultant slip is much smoother than the initial shear stress based on the amplitudes of the wavenumber spectra. We plan to feed results from the earthquake models into corresponding tsunami models to investigate tsunami generation and local propagation near the Alaska Peninsula.

REPORT

Background

Motivated by the 2011 Mw 9 Tohoku-Oki event and potential earthquakes on the Alaskan-Aleutian (A-A) Megathrust, Ryan et al. (2013) investigate the effects of realistic fault dynamics on slip, free surface deformation, and resulting tsunami formation from a Mw 9 megathrust earthquakes offshore Alaska.

Specifically, they show three scenarios: a spatially-homogenous prestress and frictional parameter model, and two models with rate-strengthening-like friction (e.g., Dieterich, 1992). Results from that study indicate adding frictional-strengthening to a region of the fault reduces both average slip and free surface displacement above the strengthening zone, with the magnitude of the reductions depending on the strengthening zone location. Additionally, corresponding tsunami models show changes in local peak amplitudes and beaming patterns for each modeled slip distribution. Given these results, other heterogeneous parameterizations, with respect to prestress and friction, still need to be examined. Andrews and Barall (2011) and Andrews and Ma (2016) specify a random prestress distribution that produces a target rupture length and moment magnitude. In those studies, the presumed stress drop tapers at the edges of the fault so that the rupture stops in a progressive fashion. A presumed mean stress drop is chosen to produce the desired moment magnitude. In addition to heterogeneous stress distributions, a more realistic fault geometry (i.e., a changing dip angle with depth) will likely affect the rupture dynamics, and this needs to be investigated further in future studies.

Completed Work

We use the elasto-dynamic finite element method (FEM) of Barall (2009) to model earthquake rupture. Generally, such FEM techniques incorporate elasticity, friction, conservation of momentum, and material properties. This is an extension of previous work by Ryan et al. (2013). In particular, we have completed several offshore Alaska models with random shear prestress distributions. The presumed stress drop tapers at the along-strike edges and at the downdip edge. The procedure, similar to Andrews and Ma (2016), is the following. In general, the procedure involves going from 2-D wavenumber space to a 2-D spatial domain via the inverse Fourier transform. First, we generate a 2-D set of complex random amplitudes with a mean of 0 and a variance of 1/2 for each real and imaginary value (so that the total variance per point, both real and imaginary, is 1):

$$\boldsymbol{\alpha} = \begin{bmatrix} \alpha_{1,1} & \alpha_{1,2} & \dots & \alpha_{1,n-1} & \alpha_{1n} \\ \alpha_{2,1} & \alpha_{2,2} & \dots & \alpha_{2,n-1} & \alpha_{2,n} \\ \vdots & \vdots & \ddots & \vdots & \vdots \\ \alpha_{n-1,1} & \alpha_{n-1,2} & \dots & \alpha_{n-1,n-1} & \alpha_{n-1,n} \\ \alpha_{n,1} & \alpha_{n,2} & \dots & \alpha_{n,n-1} & \alpha_{n,n} \end{bmatrix}$$

where α_{kl} = a+bi with a and b being real numbers and i being the imaginary unit for this n x n square matrix and where k and l are matrix indices.

Since we are dealing with wavenumber space, the structure of the wavenumber modes within the above matrix must be clarified. Wavenumbers will hold integer values. The first element of the matrix in each dimension (i.e., the top left component of the matrix) corresponds to zero wavenumber in that dimension. Wavenumbers increase in value in each dimension until the index n/2, after which the wavenumbers are negative and increase to −1 at the last element of the matrix (i.e., the bottom right component of the matrix). This type of structure comes from classic signal processing procedures. Thus, the wavenumber mapping onto α is

$$\mathbf{M} = \begin{bmatrix} (0,0) & (0,1) & \dots & (0,-2) & (0,-1) \\ (1,0) & (1,1) & \dots & (1,-2) & (1,-1) \\ \vdots & \vdots & \ddots & \vdots & \vdots \\ (-2,0) & (-2,1) & \dots & (-2,-2) & (-2,-1) \\ (-1,0) & (-1,1) & \dots & (-1,-2) & (-1,-1) \end{bmatrix}$$

where $M_{kl} = (\kappa_h, \kappa_d)$ for wavenumbers in the horizontal h and downdip d dimensions of our model fault. This wavenumber mapping should be the same size as our **α** matrix.

We modify amplitudes **α** at low wavenumber modes so that the mean value is zero – in accordance with our original statistic specification above – and so that the half-wavelength modes that correspond to the along-strike length of the fault have the largest influence on rupture propagation length. Therefore, the mean value $\alpha_{1,1}$ – corresponding to the wavenumber mode M = (0, 0) – is set to 0 + 0i. The next lowest wavenumber modes in the horizontal direction are (1, 0) and (−1, 0). These correspond to wavelengths that are the same size as the horizontal spatial dimension, and their amplitude values are each set to the value −A + 0i. Note that setting amplitudes to a negative real value will produce a positive cosine amplitude peak at the center of the spatial domain as well as a negative peak on each side via the inverse Fourier transform.

Our fault is approximately twice as large in the horizontal (i.e., along-strike) direction than in the downdip direction, and we must remove the lowest wavenumbers from the downdip dimension that are nonphysical (i.e., downdip wavelengths that are larger than

the downdip fault dimension) by setting them equal to zero. Therefore, we set the amplitudes of wavenumber modes (0, ±1), (0, ±2), (±1, ±1), and (±1, ±2) to zero. Note that we need to map these modes onto $\boldsymbol{\alpha}$ properly. We have apparently modified the statistics of our amplitude distribution at 14 modes. We have already made sure that the mean value is zero. The average variance of the modified modes is $2A^2/14$ (the sum of the squares of the amplitudes divided by the sample size), so we can ensure an average variance of 1 by setting $2A^2 = 14$, or $A = \sqrt{7}$. Now the statistics are consistent again.

A self-affine function has a 2-D Fourier transform that is proportional to the spectrum $\kappa^{-(H+1)}$ (Mandelbrot, 1977) where κ is the wavenumber and H is the Hurst exponent. For self similarity, we take H = 0. In this 2-D case, $M = (\kappa_h, \kappa_d)$ with $\kappa = (\kappa_h^2 + \kappa_d^2)^{1/2}$. Therefore we have the 2-D Fourier transform being proportional to $\kappa^{-(H+1)} = (\kappa_h^2 + \kappa_d^2)^{-(H+1)/2}$. With H = 0 our wavenumber spectrum is

$$\mathbf{S} = \begin{matrix} (0^2+0^2)^{-1/2} & (0^2+1^2)^{-1/2} & \cdots & [0^2+(-2)^2]^{-1/2} & [0^2+(-1)^2]^{-1/2} \\ (1^2+0^2)^{-1/2} & (1^2+1^2)^{-1/2} & \cdots & [1^2+(-2)^2]^{-1/2} & [1^2+(-1)^2]^{-1/2} \\ \vdots & \vdots & \ddots & \vdots & \vdots \\ [(-2)^2+0^2]^{-1/2} & [(-2)^2+1^2]^{-1/2} & \cdots & [(-2)^2+(-2)^2]^{-1/2} & [(-2)^2+(-1)^2]^{-1/2} \\ [(-1)^2+0^2]^{-1/2} & [(-1)^2+1^2]^{-1/2} & \cdots & [(-1)^2+(-2)^2]^{-1/2} & [(-1)^2+(-1)^2]^{-1/2} \end{matrix}$$

Of course the first entry above is undefined, but we can replace that entry with a somewhat arbitrary value (e.g., a value of 1) for the following computations since we have already assigned the amplitude of that entry to zero. We multiply our respective amplitudes $\boldsymbol{\alpha}$ by our desired spectrum to get $\boldsymbol{\alpha} \cdot \mathbf{S}$. Note that the first entry that results from this multiplication should be zero, since we are multiplying by zero (the lowest wavenumber mode in α was set to zero). We also apply a high wavenumber cutoff filter to reduce aliasing (incorrect high wavenumber modes resulting from the inverse Fourier transform). The Nyquist wavenumber is $\kappa = (\kappa_h^2 + \kappa_d^2)^{1/2} = n/2$ where n is the size of our matrices in each dimension. One simple Butterworth filter is $\sqrt{(1/1+(\kappa^2/\kappa_{cut}^2)^4)}$ where κ_{cut} is the cutoff wavenumber and is set to n/4 or half of the Nyquist wavenumber in this case. In matrix form, the filter is

$$\mathbf{F} = \begin{matrix} \sqrt{\frac{1}{1+\left\{\frac{(0^2+0^2)}{k_{cut}^2}\right\}^4}} & \sqrt{\frac{1}{1+\left\{\frac{(0^2+1^2)}{k_{cut}^2}\right\}^4}} & \cdots & \sqrt{\frac{1}{1+\left\{\frac{[0^2+(-2)^2]}{k_{cut}^2}\right\}^4}} & \sqrt{\frac{1}{1+\left\{\frac{[0^2+(-1)^2]}{k_{cut}^2}\right\}^4}} \\ \sqrt{\frac{1}{1+\left\{\frac{(1^2+0^2)}{k_{cut}^2}\right\}^4}} & \sqrt{\frac{1}{1+\left\{\frac{(1^2+1^2)}{k_{cut}^2}\right\}^4}} & \cdots & \sqrt{\frac{1}{1+\left\{\frac{[1^2+(-2)^2]}{k_{cut}^2}\right\}^4}} & \sqrt{\frac{1}{1+\left\{\frac{[1^2+(-1)^2]}{k_{cut}^2}\right\}^4}} \\ \vdots & \vdots & \ddots & \vdots & \vdots \\ \sqrt{\frac{1}{1+\left\{\frac{[(-2)^2+0^2]}{k_{cut}^2}\right\}^4}} & \sqrt{\frac{1}{1+\left\{\frac{[(-2)^2+1^2]}{k_{cut}^2}\right\}^4}} & \cdots & \sqrt{\frac{1}{1+\left\{\frac{[(-2)^2+(-2)^2]}{k_{cut}^2}\right\}^4}} & \sqrt{\frac{1}{1+\left\{\frac{[(-2)^2+(-1)^2]}{k_{cut}^2}\right\}^4}} \\ \sqrt{\frac{1}{1+\left\{\frac{[(-1)^2+0^2]}{k_{cut}^2}\right\}^4}} & \sqrt{\frac{1}{1+\left\{\frac{[(-1)^2+1^2]}{k_{cut}^2}\right\}^4}} & \cdots & \sqrt{\frac{1}{1+\left\{\frac{[(-1)^2+(-2)^2]}{k_{cut}^2}\right\}^4}} & \sqrt{\frac{1}{1+\left\{\frac{[(-1)^2+(-1)^2]}{k_{cut}^2}\right\}^4}} \end{matrix}$$

Accounting for the specified spectrum and filter, the modified amplitude matrix $\boldsymbol{\beta} = \boldsymbol{\alpha} \cdot \mathbf{S} \cdot \mathbf{F}$. We take the inverse Fourier transform of β and divide through by 2A to normalize the function by the sum of the absolute values of the lowest nonzero horizontal modes. This results in a random self-similar 2-D function $w(x,d) = (1/2A)F^{-1}(\boldsymbol{\beta})$, where x is the along-strike coordinate and d is the downdip coordinate, with an amplitude envelope determined by those lowest nonzero horizontal modes. We use the real part of w, although we could have equally used the imaginary part instead (note that this would have required setting the imaginary amplitudes at the lowest nonzero modes to −A). Our target along-strike rupture length is about 358 km, and the size of each matrix above is chosen to be n = 360. The single-wavelength modes (i.e., (±1,0)) have half wavelengths characterized by n/2 = 180 points so we choose a grid interval of 2 km (i.e., 180 nodes correspond to 358 km). Note that we need to consider half wavelengths since the aim is to taper the stress envelope to zero at the fault edges. The downdip length of the modeled fault is about 206 km. Therefore, we use a fault grid from w that contains the middle 180 points along the x-dimension and the top 104 points in the d-dimension. Since we have filtered the amplitudes at half of the Nyquist wavenumber (or double the Nyquist wavelength) we could suitably interpolate onto grid intervals up to 4 km. However, we use a grid interval of 2 km.

In order to implement a tapered stress drop at the most downdip extent of the fault, we use the downdip-conditioning function $C(d) = 1/[1+(d/d_0)^4]$ where d is the distance downdip and d0 is a constant used to alter the stress drop distribution downdip. Now, the shear prestress function is parameterized by $\tau_0 = [\mu_k + \gamma w(x,d)]C(d)\sigma_0$ where γ is a variable that scales w, μ_k is the kinetic (or dynamic) friction coefficient, and σ_0 is the normal prestress. Note that the shear prestress decreases as d increases due to the downdip-conditioning function. We set $\gamma = 0.2000$ and $d_0 = 143.9$ km for this study. The static friction coefficient, μ_s, is parameterized by $\mu_s = \max\{0.5630, 1.01 \cdot (\tau_0/\sigma_0)\}$ so that nucleation only occurs on a specified zone of the fault. The material properties and model parameters are listed in Table 1.

Table 1: Material properties and model parameters.

Shear Prestress (τ_0)	3.172 MPa
Normal Prestress (σ_0)	11.06 MPa
Random Shear Prestress	τ_R
Density	2670 kg/m^3
Shear Modulus	40.00 GPa
S-wave Speed	3.871 km/s
P-wave Speed	6.704 km/s
Distance Along-Strike	358.0 km
Distance Downdip	205.1 km
Fault Area	7343e1 km^2
Dip Angle	10.00°
Nucleation Radius	16.00 km
Nucleation Depth	15.50 km
Nucleation Speed	2.000 km/s
Element Size (along fault)	≈2 km
Dynamic Rupture Time Step	1.000e-2 s
Frictional Decay Time	2.600 s
Static Friction	0.5630
Static Friction (random shear prestress)	max{0.5630,1.01*(τ_R/σ_0)}
Kinetic Friction	0.1333
Kinetic Friction (strengthening)	0.3218
Hydrodynamic Grid Size	2.000 km
Hydrodynamic Time Step	1.000e-1 s

Figures 1 through 4 show four random shear prestress distributions using the process described above. Figure 5 shows the final slip distribution that results from dynamic rupture process and from the prestress distribution shown in Figure 4. Figure 6 shows the fault slip and fault shear stress spectra corresponding to Figures 4 and 5. We find that the slip spectra consists of relatively lower amplitude short wavelength (large wavenumber) components when compared to the initial shear stress spectra. However, the slip distribution does qualitatively resemble the initial shear stress distribution in that the main slip patches are near the regions of higher initial shear stress. We also note that the slip patches are shifted somewhat updip of the high initial shear stress patches. This is likely due to the free surface boundary condition - dynamic perturbations in stress causing relatively larger dynamic stress drop that is amplified as rupture travels updip along a thrust fault (Oglesby et al., 1998).

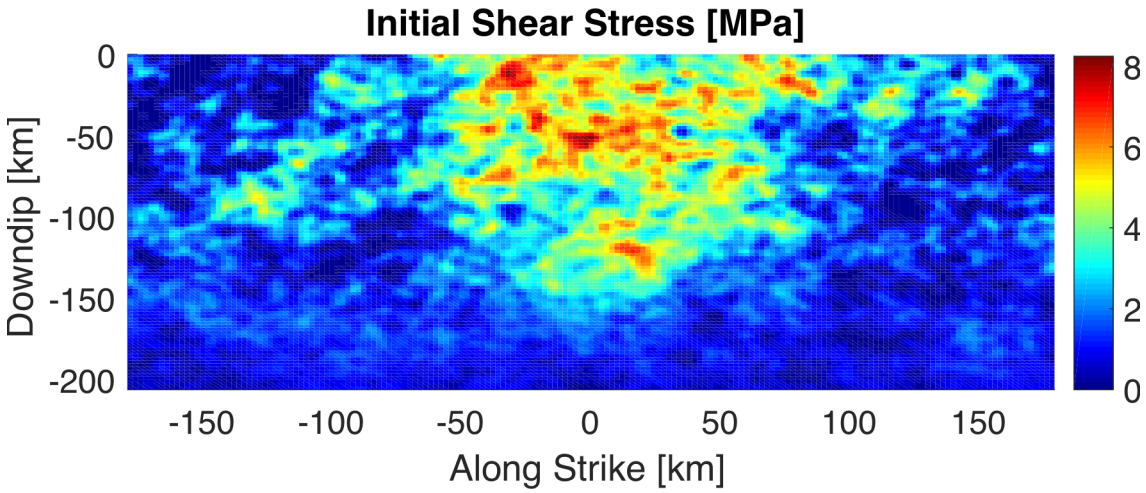

Figure 1: Randomized shear prestress distribution.

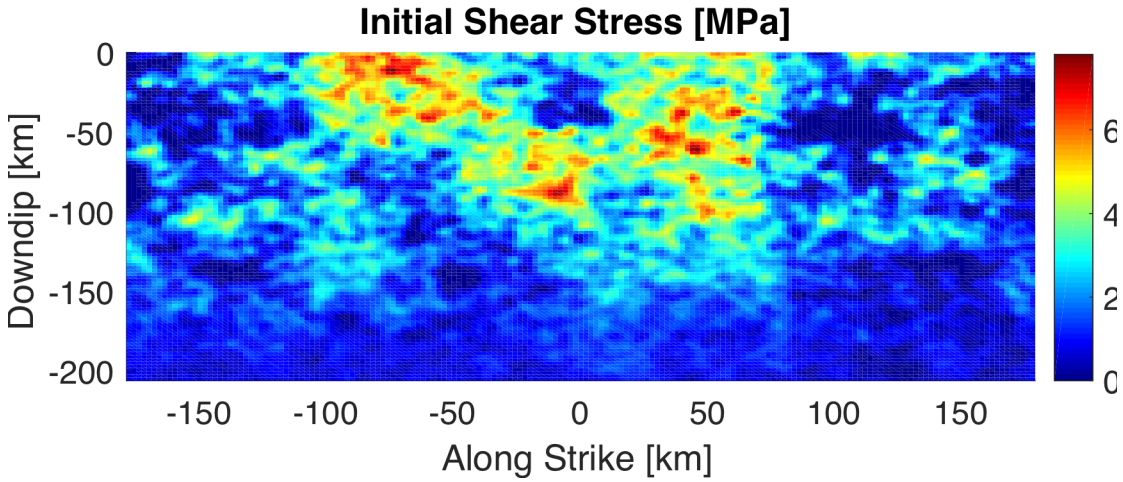

Figure 2: Randomized shear prestress distribution.

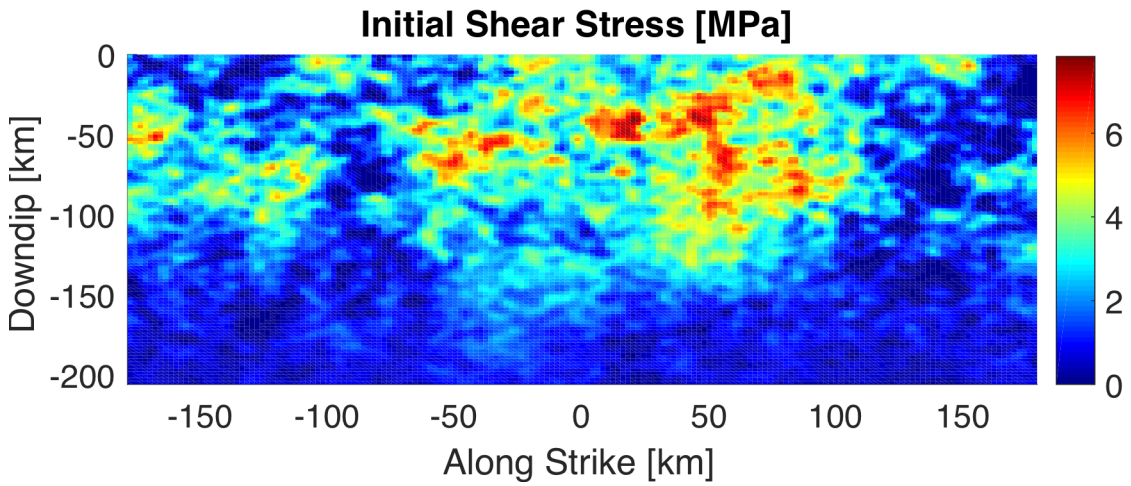

Figure 3: Randomized shear prestress distribution.

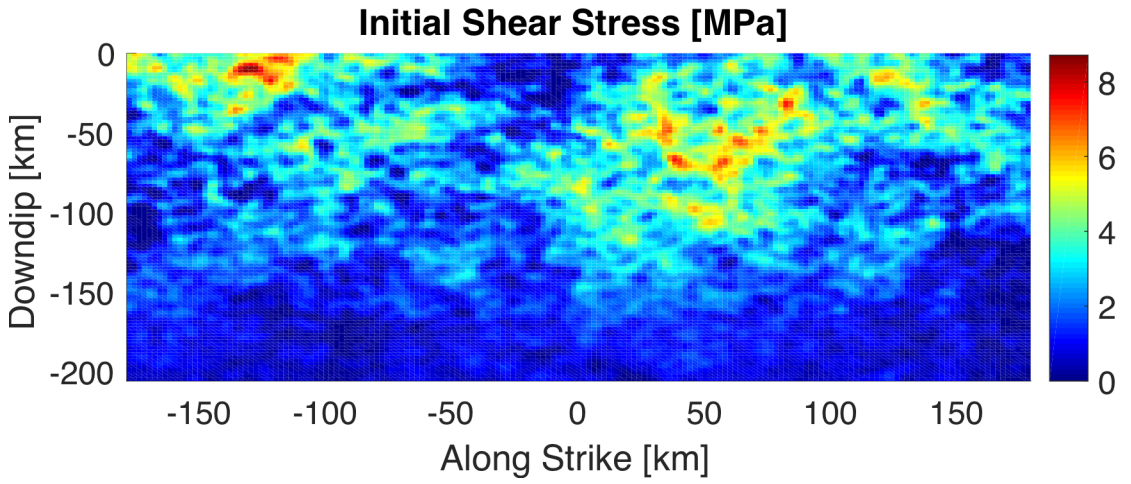

Figure 4: Randomized shear prestress distribution.

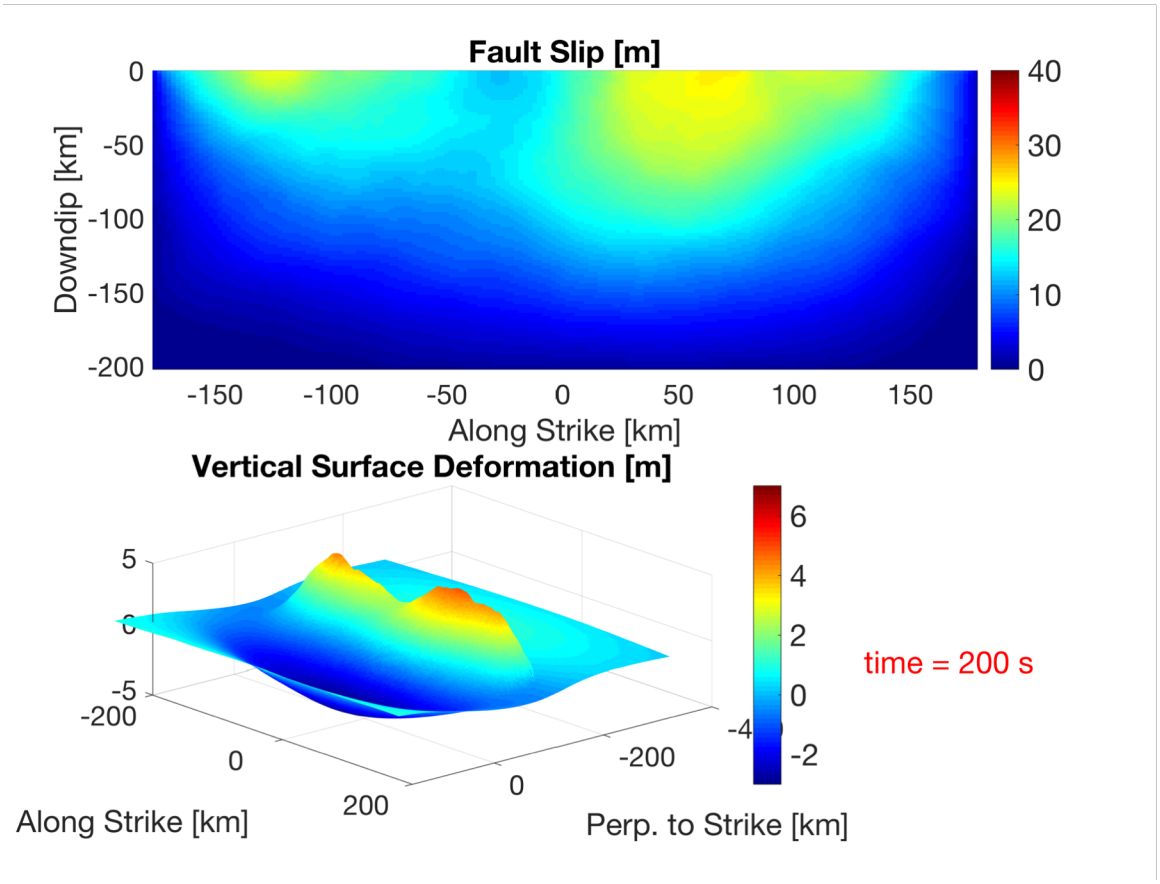

Figure 5: The shear prestress distribution from Figure 4 is used to dynamically model rupture. The resultant slip distribution is "smoother" than the initial shear stress distribution, but does show a heterogeneous pattern that qualitatively resembles the initial shear stress distribution. Further work is needed to assess wider-ranging impacts from a suite of random initial shear stress distributions.

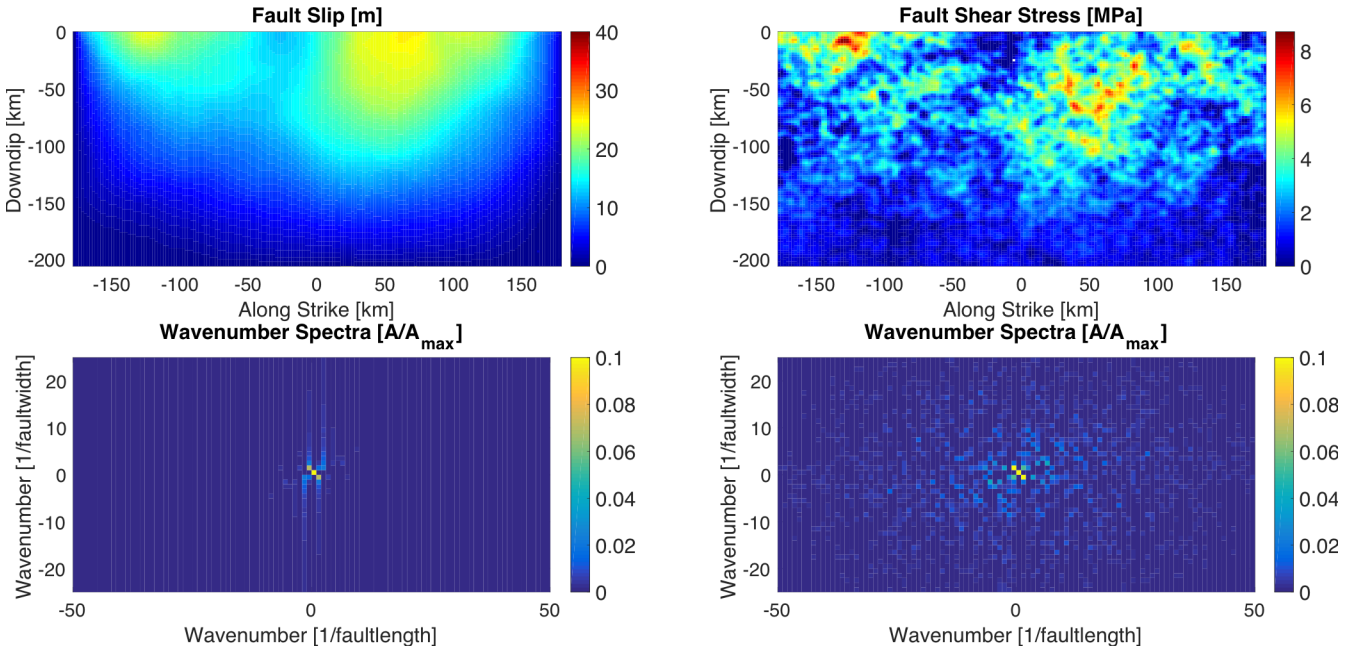

Figure 6: Fault slip and initial shear stress spectra. Using the example from Figures 4 and 5, the resultant slip distribution is smoother than the initial shear stress distribution, but does show a heterogeneous pattern that qualitatively resembles the initial shear stress distribution. The wavenumber spectra for the slip distribution is localized to relatively lower wavenumbers (i.e., larger wavelength components) than the corresponding spectra of initial shear stress.

References

Andrews, D. J. and Barall, M. (2011). Specifying initial stress for dynamic heterogeneous earthquake source models. Bull. Seismol. Soc. Am., 101(5):2408-2417.

Andrews, D. J. and Ma, S. (2016). Validating a dynamic earthquake model to produce realistic ground motion. Bull. Seismol. Soc. Am., 106(2):665– 672.

Barall, M. (2009). A grid-doubling finite-element technique for calculating dynamic three-dimensional spontaneous rupture on an earthquake fault. Geophys. J. Int., 178:845–859.

Dieterich, J. H. (1992). Earthquake nucleation on faults with rate- and state-dependent strength. J. Geophys. Res., 211:115–134.

Mandelbrot, B. B. (1977). Fractals. W. H. Freeman, San Francisco, California.

Presentations

(oral)

Ryan, Geist, Barall, and Oglesby (2016). *Dynamic Earthquake and Tsunami Modeling Offshore Ventura, California.* Southern California Earthquake Center Annual Meeting: Ventura Special Fault Study Area Workshop (Invited).

Ryan, Geist, Barall, and Oglesby (2016). *Dynamic Earthquake and Tsunami Modeling Offshore Alaska and Southern California.* University of California, Los Angeles Tectonics/Seismology Seminar (Invited).

(poster)

Ryan, Geist, Oglesby (2016). *Modeling Rupture with Heterogeneous Prestress and through Stable-Sliding Zones: Implications for an Alaskan-Aleutian Megathrust Earthquake and Tsunami.* American Geophysical Union annual conference.

Ryan, Geist, Oglesby (2017). *Modeling Rupture with Heterogeneous Prestress and through Stable-Sliding Zones: Implications for an Alaskan-Aleutian Megathrust Earthquake and Tsunami.* Seismological Society of America annual conference.

Publications are being prepared currently; none are published yet.